Classical and quantum dynamics of a model for atomic-molecular Bose-Einstein condensates

G. Santos,[1] A. Tonel,[1] A. Foerster,[1] and J. Links[2]

[1]*Instituto de Física da UFRGS, Av. Bento Gonçalves 9500, Porto Alegre, RS, Brazil*

[2]*Centre for Mathematical Physics, School of Physical Sciences, The University of Queensland, Queensland 4072, Australia*

(Received 26 October 2005; published 13 February 2006)

We study a model for a two-mode atomic-molecular Bose-Einstein condensate. Starting with a classical analysis we determine the phase space fixed points of the system. It is found that bifurcations of the fixed points naturally separate the coupling parameter space into four regions. The different regions give rise to qualitatively different dynamics. We then show that this classification holds true for the quantum dynamics.

PACS number(s): 03.75.Kk, 03.75.Hh, 05.30.Jp, 03.65.Sq

I. INTRODUCTION

Since the early experimental realizations of Bose-Einstein condensates (BECs) using alkali-metal atoms [1,2], a significant effort has been made to produce a stable BEC in a gas of molecules [3]. To our knowledge, a molecular condensate could lead to a host of new scientific investigations that includes the quantum gas with anisotropic dipolar interactions [4], the study of rotational and vibrational energy transfer processes [5], and coherent chemistry where the reactants and products are in a coherent quantum superposition of states [6], among others. In recent years the creation of a molecular BEC from an atomic BEC has been achieved by different techniques such as photoassociation [7], two-photon Raman transition [8], and Feshbach resonance [9].

From a theoretical point of view, molecular BECs may be studied using the Gross-Pitaevski (GP) equations and mean-field theory (MFT) (e.g., see Refs. [10,11]). The GP-MFT approach reduces the full multibody problem into a set of coupled nonlinear Schrödinger equations, which are then solved numerically to obtain the Josephson-type dynamics of the coupled atomic and molecular fields. An approximation can be made to reduce the complex multibody problem into a two-mode problem. An analysis of this two-mode Hamiltonian was carried out in Ref. [10], where it was established that the quantum solutions break away from the MFT predictions in the vicinity of the dynamically unstable molecular mode due to strong quantum fluctuations. It has been shown that the two-mode Hamiltonian is an exactly solvable model in the framework of the algebraic Bethe ansatz method [12] and an analysis using these results was given in Ref. [13]. However, in most of the above investigations, the atom-atom, atom-molecule, and molecule-molecule S-wave scattering interactions were not taken into account.

In the present work we focus on a more general Hamiltonian which takes into account the S-wave scattering interactions. By means of a classical analysis we first obtain the fixed points of the system and find that the space of coupling parameters divides into four distinct regions which are determined by fixed point bifurcations. By contrast, only three such regions exist when the S-wave scattering interactions are neglected. The results allow us to qualitatively predict the dynamical behavior of the system in terms of whether the evolution is localized or delocalized. Using exact diagonalization of the Hamiltonian, we then see that the quantum

dynamics within each region has a similar character.

The paper is organized as follows: In Sec. II we present the Hamiltonian and in Sec. III a classical analysis of the model is performed. In Sec. IV we investigate the quantum dynamics through the time evolution of the expectation value of the relative atom number. Section V is reserved for a discussion of the results.

II. THE MODEL

Let us consider the following general Hamiltonian, based on the two-mode approximation, describing the coupling between atomic and diatomic-molecular Bose-Einstein condensates:

$$H = U_a N_a^2 + U_b N_b^2 + U_{ab} N_a N_b + \mu_a N_a + \mu_b N_b + \Omega(a^\dagger a^\dagger b + b^\dagger aa). \tag{1}$$

Above, $a^\dagger$ is the creation operator for an atomic mode while $b^\dagger$ creates a molecular mode. The Hamiltonian commutes with the total atom number $N = N_a + 2N_b$, where $N_a = a^\dagger a$ and $N_b = b^\dagger b$. Notice that the change of variable $\Omega \to -\Omega$ is equivalent to the unitary transformation

$$b \to -b. \tag{2}$$

The parameters U_j describe S-wave scattering, taking into account the atom-atom (U_a), atom-molecule (U_{ab}), and molecule-molecule (U_b) interactions. The parameters μ_i are external potentials and Ω is the amplitude for the interconversion of atoms and molecules. In the limit $U_a = U_{ab} = U_b = 0$, (1) has been studied using a variety of methods [10,12–14]. However in the experimental context, the S-wave scattering interactions play a significant role. It will be seen below that for the general model (1) the inclusion of these scattering terms has a nontrivial consequence. We mention that generally the values for U_b and U_{ab} are unknown [6,8], although some estimates exist in the case of ^{85}Rb [11].

We finally note that the Hamiltonian (1) is a natural generalization of the two-site Bose-Hubbard model

$$H = U(N_1 - N_2)^2 + \mu(N_1 - N_2) + \Omega(a_1^\dagger a_2 + a_2^\dagger a_1) \tag{3}$$

which has been extensively studied as a model for quantum tunneling between two single-mode Bose-Einstein condensates [14–20]. Our analysis will show that despite apparent

similarities between the Hamiltonians (1) and (3), they do display some very different properties. This aspect will be discussed in Sec. V.

III. THE CLASSICAL ANALYSIS

Let N_j, θ_j, $j=a,b$ be quantum variables satisfying the canonical relations

$$[\theta_a, \theta_b] = [N_a, N_b] = 0, \quad [N_j, \theta_k] = i\delta_{jk}I.$$

Using the fact that

$$\exp(i\theta_j)N_j = (N_j + 1)\exp(i\theta_j)$$

we make a change of variables from the operators $j, j^\dagger$, $j=a,b$ via

$$j = \exp(i\theta_j)\sqrt{N_j}, \quad j^\dagger = \sqrt{N_j}\exp(-i\theta_j)$$

such that the Heisenberg canonical commutation relations are preserved. We make a further change of variables

$$z = \frac{1}{N}(N_a - 2N_b),$$

$$N = N_a + 2N_b,$$

$$\theta = \frac{N}{4}(2\theta_a - \theta_b),$$

such that z and θ are canonically conjugate variables; i.e.,

$$[z, \theta] = iI.$$

In the limit of large N we can now approximate the (rescaled) Hamiltonian by

$$H = \lambda z^2 + 2\alpha z + \beta + \sqrt{2(1-z)}(1+z)\cos\left(\frac{4\theta}{N}\right) \quad (4)$$

with

$$\lambda = \frac{\sqrt{2N}}{\Omega}\left(\frac{U_a}{2} - \frac{U_{ab}}{4} + \frac{U_b}{8}\right),$$

$$\alpha = \frac{\sqrt{2N}}{\Omega}\left(\frac{U_a}{2} - \frac{U_b}{8} + \frac{\mu_a}{2N} - \frac{\mu_b}{4N}\right),$$

$$\beta = \frac{\sqrt{2N}}{\Omega}\left(\frac{U_a}{2} + \frac{U_{ab}}{4} + \frac{U_b}{8} + \frac{\mu_a}{N} + \frac{\mu_b}{2N}\right),$$

where, since N is conserved, we treat it as a constant. We note that the unitary transformation (2) is equivalent to $\theta \rightarrow \theta + N\pi/4$. Also, since the Hamiltonian (1) is time-reversal invariant, we will hereafter restrict our analysis to the case $\lambda \geq 0$.

We now regard Eq. (4) as a classical Hamiltonian and investigate the fixed points of the system. The first step is to find Hamilton's equations of motion which yield

$$\frac{dz}{dt} = \frac{\partial H}{\partial \theta} = -\frac{4}{N}\sqrt{2(1-z)}(1+z)\sin\left(\frac{4\theta}{N}\right),$$
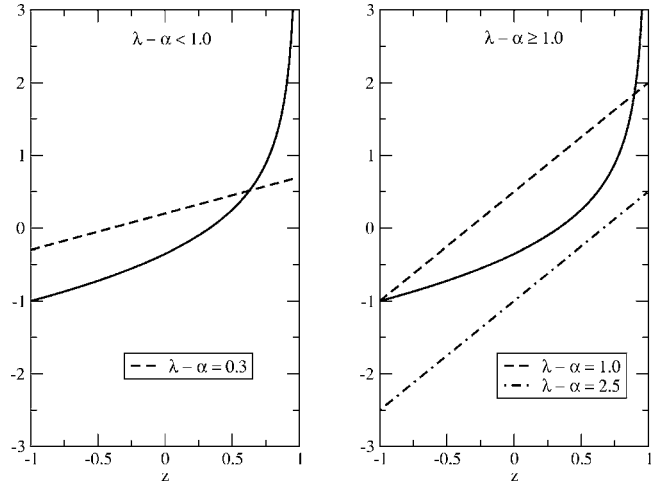

FIG. 1. Graphical solution of Eq. (6). The crossing between the straight line [left-hand side of Eq. (6)] and the curve [right-hand side of Eq. (6)] for different $\lambda - \alpha$ values represents the solution(s) for each case. There is just one solution on the left ($\lambda - \alpha < 1$), while there are either two solutions or no solution on the right ($\lambda - \alpha \geq 1$).

$$-\frac{d\theta}{dt} = \frac{\partial H}{\partial z} = 2\lambda z + 2\alpha + \frac{1 - 3z}{\sqrt{2(1-z)}}\cos\left(\frac{4\theta}{N}\right).$$

The fixed points of the system are determined by the condition

$$\frac{\partial H}{\partial \theta} = \frac{\partial H}{\partial z} = 0. \quad (5)$$

Due to the periodicity of the solutions, below we restrict to $\theta \in [0, N\pi/2]$. This leads to the following classification:

$\theta = N\pi/4$, and z is a solution of

$$\lambda z + \alpha = \frac{1 - 3z}{2\sqrt{2(1-z)}}$$

which has no solution for $\lambda - \alpha < -1$ while there is a unique locally minimal solution for $\lambda - \alpha \geq -1$.

$\theta = 0$, and z is a solution of

$$\lambda z + \alpha = \frac{3z - 1}{2\sqrt{2(1-z)}} \quad (6)$$

which has a unique locally maximal solution for $\lambda - \alpha < 1$ while for $\lambda - \alpha > 1$ there are either two solutions (one locally maximal point and one saddle point) or no solutions. In Fig. 1 we present a graphical solution of Eq. (6).

$z = -1$ and θ is a solution of

$$\cos\left(\frac{4\theta}{N}\right) = \lambda - \alpha$$

for which there are two saddle point solutions for $|\lambda - \alpha| < 1$.

It is also useful to identify the points $z=1, \theta=N\pi/8$, and $z=1, \theta=3N\pi/8$, where the singular derivative $\partial H/\partial z$ changes sign. For $z=1$ the Hamiltonian (4) is independent of θ, so these points essentially behave like a saddle point. We re-
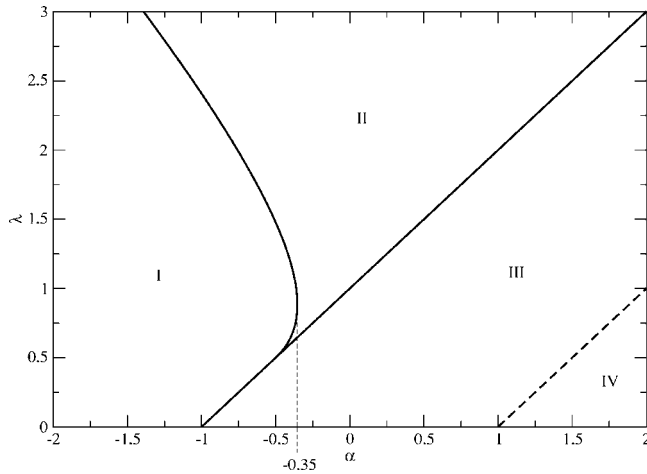
FIG. 2. Parameter space diagram identifying the different types of solution for Eq. (5). In region I there are no solutions for z when $\theta=0$, and one solution for z when $\theta=N\pi/4$. In region II there are two solutions for z when $\theta=0$, and one solution for z when $\theta=N\pi/4$. In region III exists one solution for z when $\theta=0$, one solution for z when $\theta=N\pi/4$, and two solutions for θ when $z=-1$. In region IV there is one solution for z when $\theta=0$, and no solution for z when $\theta=N\pi/4$. The boundary separating regions II and III is given by $\lambda=\alpha+1$, while the equation $\lambda=\alpha-1$ separates the regions III and IV. The boundary between regions I and II has been obtained numerically.

mark that Eq. (4) is also independent of θ for $z=-1$.

From the above we see that there exist fixed point bifurcations for certain choices of the coupling parameters. These bifurcations allow us to divide the parameter space into four regions, as depicted in Fig. 2. The asymptotic form of the boundary between regions I and II is discussed in the Appendix.

To visualize the dynamics, it is useful to plot the level curves of the Hamiltonian (4). Since the fixed point bifurcations change the topology of the level curves, qualitative differences can be observed between each of the four regions. The results are shown in Figs. 3 and 4, where for clarity we now take $4\theta/N \in [-2\pi, 2\pi]$.

Figure 3(a) shows the typical character of the level curves in region I. The maximal level curve occurs along the phase space boundary $z=-1$ and there are two local minima. Note that for no choice of parameters do these minima occur on the boundary $z=1$, but they may occur arbitrarily close to this boundary. If the initial state of the system has $z\approx 1$ then z will remain close to 1 for all subsequent times. A similar situation is true if the initial state of the system has $z\approx-1$. For both cases we see that the evolution of the system is localized.

As the coupling parameters are changed and the system crosses the boundary into region II, two new fixed points, a maxima and a saddle point, emerge at $\theta=0$ which can happen for any $z\in[-1,1)$. On crossing this parameter space boundary the maximum may move towards the phase space boundary $z=1$ while the saddle point approaches $z=-1$. Also the two minima may move away from the phase space boundary $z=-1$, as depicted in Fig. 3(b). The consequence for the dynamics is that for an initial state with $z\approx-1$ the
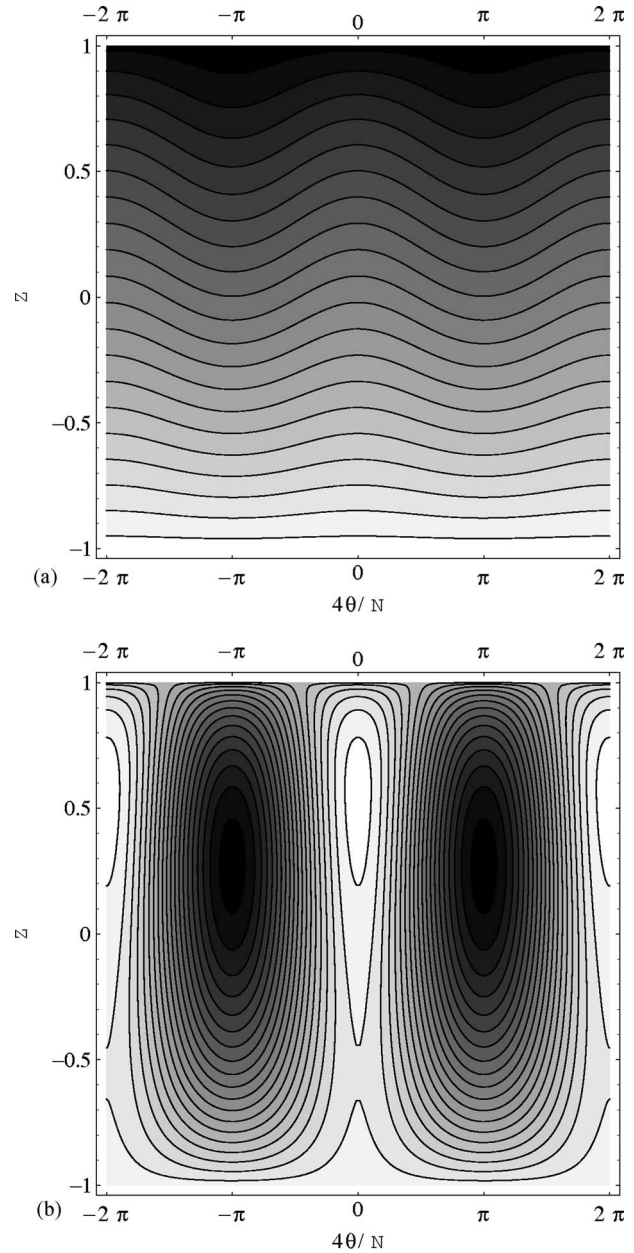

FIG. 3. Level curves of the Hamiltonian (4) in (a) region I and (b) region II. The parameter values are $\lambda=1.0, \alpha=-8.0$ for region I and $\lambda=1.0, \alpha=-0.2$ for region II. In region I we observe the presence of local minima for $4\theta/N=\pm\pi$. Besides the minima at $4\theta/N=\pm\pi$, two additional fixed points (a maximum and a saddle point) are apparent in region II occurring at $\theta=0$.

evolution of the system is still localized, but for an initial state with $z\approx 1$ the evolution is delocalized.

Figure 4(a) illustrates what happens when the coupling parameters are tuned to cross over from region II into region III. The saddle point at $\theta=0$ approaches $z=-1$, reaching the phase space boundary exactly when the coupling parameters lie in the boundary between regions II and III. The saddle point then undergoes a bifurcation into two saddle points occurring at $z=-1$ for different values of θ in region III. The two mimima have also moved away from $z=1$ towards $z=$
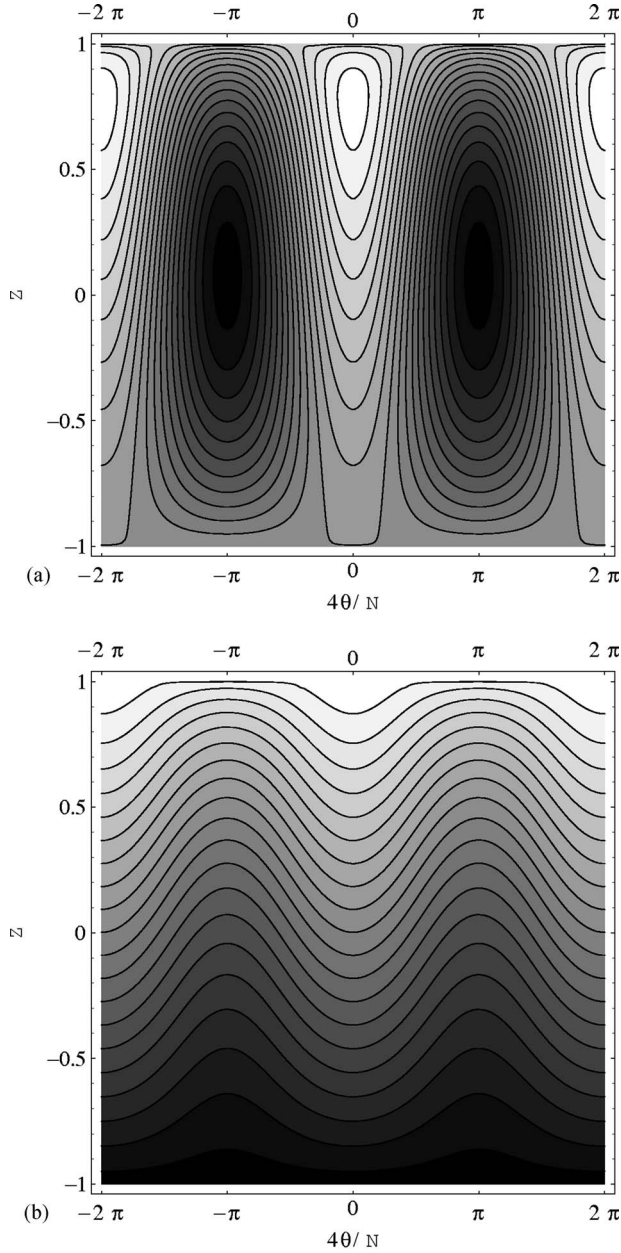
FIG. 4. Level curves of the Hamiltonian (4) in (a) region III and (b) region IV. The parameter values are $\lambda=1.0, \alpha=0.2$ on the left and $\lambda=1.0, \alpha=3.0$ on the right. In region III we observe the presence of minima at $4\theta/N=\pm\pi$ and for $\theta=0$ just one fixed point, a maximum. There are also saddle points for when $z=-1$. In region IV just one fixed point (a maximum) occurs for $\theta=0$, which always has $z<1$. In contrast the global minimum occurs for $z=-1$.

-1. Now the dynamics is delocalized for both initial states $z\approx1$ and $z\approx-1$.

It is also possible to tune the parameters to move from region I directly to region III. At the boundary between the regions, a single local maximum emerges from the point $z=-1$, $\theta=0$. As the parameters are tuned to move away from the boundary into region III, the maximum moves towards $z=1$ while the minima at $\theta=\pm N\pi/4$ approaches $z=-1$.

Moving from region III towards region IV causes the two saddle points for $z=-1$ to move towards $\theta=\pm N\pi/4$. Again,

the two minima for $\theta=\pm N\pi/4$ move towards $z=-1$. Each minimum converges with a saddle point exactly when the coupling parameters are on the boundary of regions III and IV. Varying the coupling parameters further into region IV we find that minima for the Hamiltonian are always at $z=-1$, $\theta=\pm N\pi/4$, and the local maximum for $\theta=0$ lies close to $z=1$, as shown in Fig. 4. For this case the dynamics is localized for both initial states $z\approx1$ and $z\approx-1$.

The above discussion gives a general qualitative description of the dynamical behavior of the classical system in terms of the four regions identified in the parameter space. We emphasize that the change in the classical dynamics as the boundary between two regions is crossed is *smooth*. Nonetheless, the analysis does give a useful insight into the possible general dynamical behaviors. Below we will show that the same holds true for the quantum dynamics.

IV. QUANTUM DYNAMICS

Having analyzed the classical dynamics, we now want to investigate the extent to which a similar scenario holds for the quantum system. For the case $\lambda=0$ (where the coupling for all S-wave scattering interactions is zero) the quantum dynamics has previously been studied in Refs. [10,13]. In this instance region II is not accessible. It was shown that the dynamics is delocalized for $|\alpha|<1$ and localized otherwise for both atomic and molecular inital states, consistent with the classical results described above. A surprising aspect of the classical analysis is the existence of region II where the evolution of a purely molecular inital state is highly localized, whereas the evolution of a purely atomic initial state is completely delocalized. We will see that this also occurs for the quantum case. Thus the inclusion of the S-wave scattering interactions into the Hamiltonian gives richer dynamics.

The time evolution of any state is given by $|\Psi(t)\rangle = U(t)|\phi\rangle$, where $U(t)$ is the temporal operator $U(t) = \sum_{m=0}^{M}|m\rangle\langle m|\exp(-iE_m t)$, $|m\rangle$ is an eigenstate with energy E_m, and $|\phi\rangle=|N_a,N_b\rangle$ represents the initial Fock state with N_a atoms and N_b molecules such that $N_a+2N_b=N$. We adopt the method of directly diagonalizing the Hamiltonian as done in [19,20] for the Bose-Hubbard Hamiltonian (3) and compute the expectation value of the relative number of atoms

$$\langle N_a(t) - 2N_b(t)\rangle = \langle\Psi(t)|N_a - 2N_b|\Psi(t)\rangle$$

using two different initial state configurations: a purely atomic state and a purely molecular state. Hereafter, we will fix the following parameters $N=100$, $\Omega=1.0$, $\mu_a=0.0$, $\mu_b=0.0$, and $U_b=1.0$.

In Fig. 5 we plot the expectation value of the relative number of atoms for $\lambda=1.0$ and the choices $\alpha=-8.0$, -0.2, 0.2, and 3. The graphs depict the quantum dynamics for those cases where the system is in regions I, II, III, and IV from top to bottom, respectively. On the left we are using a purely atomic initial state $|N,0\rangle$ and on the right-hand side a purely molecular initial state $|0,N/2\rangle$.

Figure 5 displays aspects of the quantum dynamics, such as the collapse and revival of oscillations and nonperiodic oscillations, which are not features of the corresponding classical dynamics [cf. [15] for analogous results for the Hamil-
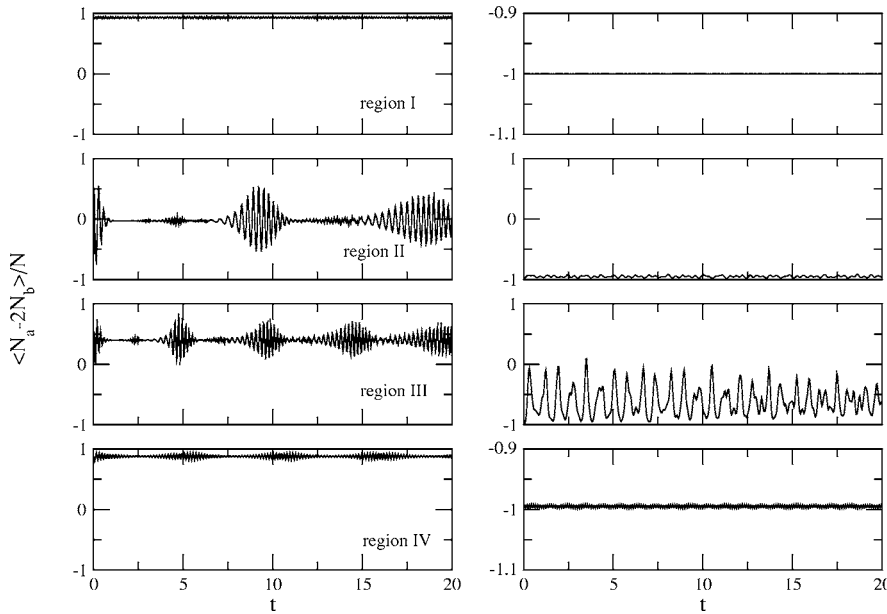
FIG. 5. Time evolution of the expectation value of the imbalance population $\langle N_a - 2N_b \rangle / N$ in the four regions defined by the diagram with a purely atomic initial state $|N,0\rangle$ on the left and a purely molecular initial state $|0,N/2\rangle$ on the right. We are using $\lambda = 1.0$ and $\alpha = -8.0, -0.2, 0.2, 3.0$ (or, in terms of the original variables, $U_b = 1, U_a = -0.881, 0.222, 0.278, 0.674$ and $U_{ab} = -1.546, 0.660, 0.774, 1.566$).

tonian (3)]. However, it also shows that the classification based on classical fixed point bifurcations to determine whether the dynamic evolution is localized or delocalized applies to the quantum case. In particular, in region II it is clear that for an initial atomic state the evolution is completely delocalized, but localized for an initial molecular state.

V. DISCUSSION

Using the classical Hamiltonian (4) as an approximation to the quantum Hamiltonian (1), we have undertaken an analysis to determine the fixed points of the system. The bifurcations of the fixed points divide the coupling parameter space into different regions characterizing different dynamics, which can also be seen for the quantum dynamics. It is necessary to establish the extent to which the classical approximation is valid. Since λ and α vary with the number of particles, it is required that the gap between successive energy levels should approach a continuum for large N. This imposes that $\lambda, \alpha \ll N^{3/2}$. We can compare this situation to the case of the Bose-Hubbard model (3), where a similar classical analysis is valid for $|U/\Omega| \ll N$ [17]. It was shown in Ref. [20] that for that model there are transitions in the dynamical behavior for the quantum regime $|U/\Omega| \gg N$, which are not apparent from the classical analysis. These properties were found to be closely related to couplings for when the energy gap between the ground and first excited state was minimal or maximal. We should expect a similar result to occur for Eq. (1).

The relationship between fixed point bifurcations and ground-state entanglement has been studied in Ref. [25]. There it was argued that the ground-state entanglement of a quantum system will be maximal whenever the classical system undergoes a supercritical pitchfork bifurcation for the lowest energy in phase space. A peak in a measure of the ground-state entanglement has been shown in many instances to be indicative of a quantum phase transition [21–23]. For the Hamiltonian (1) we have considered here, there are no supercritical pitchfork bifurcations. For $\lambda = 0$ there is a quantum phase transition at $\alpha = 1$, as can be seen from the behavior of certain ground-state correlation functions [11,13,14]. This does correspond to a bifurcation of the lowest energy in phase space. Calculation of the ground-state entanglement in this case have been undertaken in Ref. [14], showing that it is maximal at a coupling different from the critical point.

This is in some contrast to the Bose-Hubbard model (3). There, a supercritical pitchfork bifurcation of the lowest energy occurs in the *attractive* case [18,20], and the results of Ref. [24] suggest that indeed the entanglement is maximal at this coupling. (For the repulsive case the ground-state entanglement is a smooth, monotonic function of the coupling [14].) However, the transition from localization to delocalization for the dynamics as studied in Refs. [15,19,20] does not occur at the bifurcation. Despite the apparent similarities between Eqs. (1) and (3), we can see that the interrelationship between bifurcations of the classical system and properties of the quantum system are very different.

APPENDIX

In this Appendix we analyze the boundary dividing regions I and II. In particular, we determine the asymptotic

relation between λ and α when λ is large and when λ is close to $\frac{1}{2}$. We also compute the maximum value of α on this boundary.

Consider

$$f(z) = \lambda z + \alpha,$$

$$g(z) = \frac{3z - 1}{2\sqrt{2(1 - z)}},$$

where the fixed points occur when $f(z) = g(z)$. We want to determine the boundary between the cases when there is no solution and two solutions. This boundary is given by the case when $f(z)$ is the tangent line to $g(z)$. Now

$$\frac{dg}{dz} = \frac{1}{2\sqrt{2}}\left[3(1 - z)^{-1/2} + \frac{1}{2}(3z - 1)(1 - z)^{-3/2}\right]$$

so z is determined by the condition

$$\lambda = \frac{dg}{dz}. \tag{A1}$$

Below we consider three cases:

(i) First put $z = -1 + u$, where u is small and positive. Then

$$\frac{dg}{dz} \sim \frac{1}{2} + \frac{3}{16}u.$$

Solving for u gives

$$u \sim \frac{8}{3}(2\lambda - 1).$$

Now we need

$$f(z) = g(z),$$

$$\lambda(-1 + u) + \alpha = \frac{1}{2\sqrt{2}}(-4 + 3u)(2 - u)^{-1/2} \sim -1 + \frac{1}{2}u.$$

We can substitute in u to find a relation between λ and α:

$$\alpha \sim -\frac{1}{2} + \left(\lambda - \frac{1}{2}\right) - \frac{16}{3}\left(\lambda - \frac{1}{2}\right)^2.$$

This curve is valid for $\left(\lambda - \frac{1}{2}\right)$ positive. Also

$$\left.\frac{d\alpha}{d\lambda}\right|_{\lambda = 1/2} = 1$$

so the curve separating regions II and III is tangential to the curve separating regions I and III at $\lambda = \frac{1}{2}$.

(ii) Next we look at the case when $z = 1 - u$ with u small and positive. Here we find

$$g = \frac{2 - 3u}{2\sqrt{2u}},$$

$$\sim \frac{1}{\sqrt{2u}},$$

$$\frac{dg}{dz} \sim \frac{1}{2\sqrt{2}u^{3/2}},$$

so that

$$u \sim \frac{1}{2}\lambda^{-2/3}.$$

This leads to

$$\alpha = g(z) - \lambda z \sim -\lambda + \frac{3}{2}\lambda^{1/3}. \tag{A2}$$

The asymptotic equation (A2) is valid for large positive values of λ.

(iii) To complete the picture, finally we investigate the maximum of α with respect to λ. From Eqs. (A1) and (A2) we have

$$\frac{d\alpha}{d\lambda} = \frac{dg}{dz}\frac{dz}{d\lambda} - \lambda\frac{dz}{d\lambda} - z \tag{A3}$$

$$= -z \tag{A4}$$

so the maximum occurs at $z = 0$. Looking at the asymptotic behavior around $z = 0$ we have

$$g(z) \sim -\frac{1}{2\sqrt{2}}\left(1 - \frac{5}{2}z - \frac{9}{8}z^2\right),$$

$$\frac{dg}{dz} \sim -\frac{5}{4\sqrt{2}}\left(1 + \frac{9}{10}z\right),$$

which gives

$$z \sim \frac{10}{9}\left(\frac{4\sqrt{2}}{5}\lambda - 1\right).$$

Using this we can find an expression for α in terms of λ:

$$\alpha \sim -\frac{1}{2\sqrt{2}} - \frac{25}{36\sqrt{2}}\left(\frac{4\sqrt{2}}{5}\lambda - 1\right)^2.$$

The first term above corresponds to the maximal value of $\alpha \approx -0.35$ as depicted in Fig. 2.

[1] E. A. Cornell and C. E. Wieman, Rev. Mod. Phys. **74**, 875 (2002).

[2] J. R. Anglin and W. Ketterle, Nature (London) **416**, 211 (2002).

[3] P. Zoller, Nature (London) **417**, 493 (2002).

[4] K. Góral, L. Santos, and M. Lewenstein, Phys. Rev. Lett. **88**, 170406 (2002).

[5] J. T. Bahns, W. C. Stwalley, and P. L. Gould, J. Chem. Phys. **104**, 9689 (1998).

[6] D. J. Heinzen, R. Wynar, P. D. Drummond, and K. V. Kheruntsyan, Phys. Rev. Lett. **84**, 5029 (2000).

[7] N. Vanhaecke, W. de Souza Melo, B. L. Tolra, D. Comparat,

and P. Pillet, Phys. Rev. Lett. **89**, 063001 (2002).

[8] R. Wynar, R. S. Freeland, D. J. Han, C. Ryu, and D. J. Heinzen, Science **287**, 1016 (2000).

[9] E. A. Donley, N. R. Claussen, S. T. Thompson, and C. E. Wieman, Nature (London) **417**, 529 (2002).

[10] A. Vardi, V. A. Yurovsky, and J. R. Anglin, Phys. Rev. A **64**, 063611 (2001).

[11] B. J. Cusack, T. J. Alexander, E. A. Ostrovskaya, and Y. S. Kivshar, Phys. Rev. A **65**, 013609 (2002).

[12] J. Links, H.-Q. Zhou, R. H. McKenzie, and M. Gould, J. Phys. A **36**, R63 (2003).

[13] H.-Q. Zhou, J. Links, and R. H. McKenzie, Int. J. Mod. Phys. B **17**, 5819 (2003).

[14] A. P. Hines, R. H. McKenzie, and G. J. Milburn, Phys. Rev. A **67**, 013609 (2003).

[15] G. J. Milburn, J. Corney, E. E. Wright, and D. F. Walls, Phys. Rev. A **55**, 4318 (1997).

[16] S. Raghavan, A. Smerzi, and V. M. Kenkre, Phys. Rev. A **60**, R1787 (1999).

[17] A. J. Leggett, Rev. Mod. Phys. **73**, 307 (2001).

[18] S. Kohler and F. Sols, Phys. Rev. Lett. **89**, 060403 (2002).

[19] A. P. Tonel, J. Links, and A. Foerster, J. Phys. A **38**, 1235 (2005).

[20] A. P. Tonel, J. Links, and A. Foerster, J. Phys. A **38**, 6879 (2005).

[21] T. J. Osborne and M. A. Nielsen, Phys. Rev. A **66**, 032110 (2002).

[22] A. Osterloh, L. Amico, G. Falci, and R. Fazio, Nature (London) **416**, 608 (2002).

[23] G. Vidal, J. I. Latorre, E. Rico, and A. Kitaev, Phys. Rev. Lett. **90**, 227902 (2003).

[24] F. Pan and J. P. Draayer, Phys. Lett. A **339**, 403 (2005).

[25] A. P. Hines, R. H. McKenzie, and G. J. Milburn, Phys. Rev. A **71**, 042303 (2005).